

Effects of Position and Quantity of the Cyano Group in Organic Electrode Materials on Electrochemical Performance

Yongkang An,^[a] Yu Liu,^[a] Fangyu Xiong,^{*[a]} and Qinyou An^{*[a, b]}

Recently, organic cathodes have received wide attention as eco-friendly and sustainable materials for aqueous Zn-organic batteries. However, the low voltage limits its further development and the related optimization strategies are rarely reported. Herein, three HATN-based cathode materials containing cyano groups (named O3CN, P3CN, and P6CN) are proposed to reveal the role of cyano groups. The number of cyano groups was positively correlated with the potential, and the position of

cyano groups would affect the ion mobility through the steric effect. Furthermore, the cyano group also reduces the solubility of the materials in water, greatly improving the cycle stability under low current density. As a result, the average voltage increased from 0.48 V for HATN to 0.73 V for P6CN, and the capacity retained 88.2% after 5000 cycles at 5 Ag⁻¹. This study provides a systematic reference for the improvement of the voltage of organic cathode materials in the future.

Introduction

Traditional lithium-ion batteries have been developed for decades and successfully used in electric vehicles and large-scale energy storage devices, however, the emergence of lithium resource shortage, high cost, and safety issues has greatly limited the development of lithium-ion batteries.^[1] Therefore, there is an urgent need to develop next-generation rechargeable batteries.^[2] Among the various rechargeable batteries, aqueous zinc ion batteries have attracted widespread attention due to their high safety, abundant resources, low cost, and environmental friendliness.^[3] Moreover, zinc metal can be directly used as an anode and has a high theoretical capacity of 820 mAhg⁻¹.^[4] However, the redox potential (-0.76 V vs. SHE) is much higher than that of lithium (-3.04 V vs. SHE),^[4c,5] which requires a cathode with high redox potential. Therefore, the choice of the cathode material is crucial to attaining high-voltage zinc ion batteries.^[6]

The structure of the cathode material plays a decisive role in the energy density and cycle life of the whole battery.^[7] Various inorganic cathode materials have been extensively studied such as vanadium (V)-based compounds,^[8] MnO₂,^[9] and Prussian blue analogs.^[10] However, most of them have poor

cycling stability due to dissolution and structural deterioration, which makes the cost of large-scale energy storage devices dramatically higher. Organic electrode materials have recently attracted more and more interest from researchers, which is attributed to their advantages such as structural diversity, green materials, and considerable performance.^[11] In the past few years, a large number of organic cathode materials have been developed for aqueous zinc ion batteries, such as C4Q,^[12] tetrachlorobenzoquinone,^[13] PTO,^[14] PANI,^[15] DTT,^[16] TAPQ,^[17] TBQPH,^[18] HAQ-COF,^[19] etc. Among them, hexaazatrinnaphthalene (HATN) is one of the best-known materials due to its high theoretical specific capacity (418 mAhg⁻¹) and excellent cycling stability.^[20] However, the average working voltage of the battery assembled with Zn anode is only 0.48 V at 0.1 Ag⁻¹, which greatly limits its further application. To obtain higher average voltages, the researchers optimized their energy levels by the strategy of introducing strong electron-absorbing groups into the molecular structure. For example, Chen et al. adopted introducing carbonyl groups (both as active units and strong electron-withdrawing groups) into the structure, which not only improved the voltage (0.63 V at 0.1 Ag⁻¹) but also the theoretical capacity of electrode material.^[18,21] Ye et al. reduced the highest occupied molecular orbital/the lowest unoccupied molecular orbital (HOMO/LUMO) energy level of the material by introducing cyano groups ($-CN$) in the para-position, thus improving the average potential (0.62 V vs. Zn²⁺/Zn) of the battery.^[22] This method is a promising strategy for materials with numerous modifiable positions. However, systematic studies have rarely reported on the introduced position and number of the strong electron-withdrawing group.

Herein, we introduced a different quantity of $-CN$ at the ortho-position (o position) and para-position (p position) of HATN and prepared three electrode materials named O3CN, P3CN, and P6CN for aqueous zinc ion batteries. Through these four materials, the effect of the number and position of $-CN$ on the electrochemical properties was systematically investigated.

[a] Y. An, Y. Liu, Dr. F. Xiong, Prof. Q. An
State Key Laboratory of Advanced Technology for Materials Synthesis and Processing
Wuhan University of Technology
Wuhan 430070 (P. R. China)
E-mail: xiongyf0624@163.com
anqinyou86@whut.edu.cn

[b] Prof. Q. An
Hubei Longzhong Laboratory
Wuhan University of Technology (Xiangyang Demonstration Zone)
Xiangyang, Hubei, 441000 (China)

 Supporting information for this article is available on the WWW under
<https://doi.org/10.1002/batt.202200463>

 An invited contribution to a Special Collection on Organic Batteries

Combing DFT calculations and electrochemical analysis, it is obvious that the introduction of the strong electron-withdrawing group (cyano group) effectively improves the intrinsic redox potential of the material by lowering the energy level and reducing the band gap, and the degree of improvement is positively related to the amount of cyano group introduced. Furthermore, improper placement will result in a steric effect, resulting in reduced ion mobility, which will affect the electrochemical performance. As a result, the batteries assembled by P6CN achieved a higher average voltage (0.73 vs. 0.48 V) compared to HATN. In addition, the specific capacity of P6CN reached 252.7 mAh g⁻¹ after 200 cycles at 0.3 A g⁻¹, and no significant capacity degradation was observed. At a high current density of 5 A g⁻¹, the P6CN retains 88.2% of its initial value after 5000 cycles. Finally, electrochemical kinetics were revealed through a variety of characterizations.

Results and Discussion

First, the four materials (Figure 1a) were synthesized according to the previous literature through simple amino and carbonyl dehydration condensation reactions.^[18,20] The detailed synthesis processes are placed in the Supporting Information (Supporting Information, Figures S1–S4). ¹H nuclear magnetic resonance (¹H NMR) spectroscopy was used to reveal the molecular structures of the four products (Figures S5–S8). The chemical shifts of HATN and P3CN are consistent with those reported in the literature.^[20,22] For O3CN and P6CN, there are three chemical shift peaks (δ 8.91, 8.83, and 8.31) and one chemical shift peak (δ 9.51) in ¹H NMRs, respectively, indicating that the two new structures have been successfully synthesized. Fourier transforms infrared (FTIR) spectroscopy was carried out to analyze the functional group information of materials as shown in Figure 1(b). The peak located at about 2231 cm⁻¹ is observed in spectra of O3CN, P3CN, and P6CN, which belong to the vibration of the –CN bond.^[22] The peaks located at around 1510 cm⁻¹ can be attributed to the vibration of the –C=N– bond.^[20] Subsequently, two distinct peaks are shown at 1560 and 2250 cm⁻¹ of the Raman spectra (Figure 1c), which are assigned to the –C=N– and –CN bonds, respectively.^[23] The above characterizations prove that the four materials were successfully prepared. The powder of HATN, O3CN, P3CN, and P6CN are tested respectively by XRD as shown in Figure S9. All four materials exhibited good crystallinity. In addition, scanning electron microscopy (SEM) was carried out in order to characterize the micro-morphology of the materials as shown in Figure 1(d–g) and Figure S10. HATN consists of ultra-long nanowires with a diameter of 500 nm, which is consistent with the previous report.^[20] The O3CN presents an irregular plate-

NMR) spectroscopy was used to reveal the molecular structures of the four products (Figures S5–S8). The chemical shifts of HATN and P3CN are consistent with those reported in the literature.^[20,22] For O3CN and P6CN, there are three chemical shift peaks (δ 8.91, 8.83, and 8.31) and one chemical shift peak (δ 9.51) in ¹H NMRs, respectively, indicating that the two new structures have been successfully synthesized. Fourier transforms infrared (FTIR) spectroscopy was carried out to analyze the functional group information of materials as shown in Figure 1(b). The peak located at about 2231 cm⁻¹ is observed in spectra of O3CN, P3CN, and P6CN, which belong to the vibration of the –CN bond.^[22] The peaks located at around 1510 cm⁻¹ can be attributed to the vibration of the –C=N– bond.^[20] Subsequently, two distinct peaks are shown at 1560 and 2250 cm⁻¹ of the Raman spectra (Figure 1c), which are assigned to the –C=N– and –CN bonds, respectively.^[23] The above characterizations prove that the four materials were successfully prepared. The powder of HATN, O3CN, P3CN, and P6CN are tested respectively by XRD as shown in Figure S9. All four materials exhibited good crystallinity. In addition, scanning electron microscopy (SEM) was carried out in order to characterize the micro-morphology of the materials as shown in Figure 1(d–g) and Figure S10. HATN consists of ultra-long nanowires with a diameter of 500 nm, which is consistent with the previous report.^[20] The O3CN presents an irregular plate-

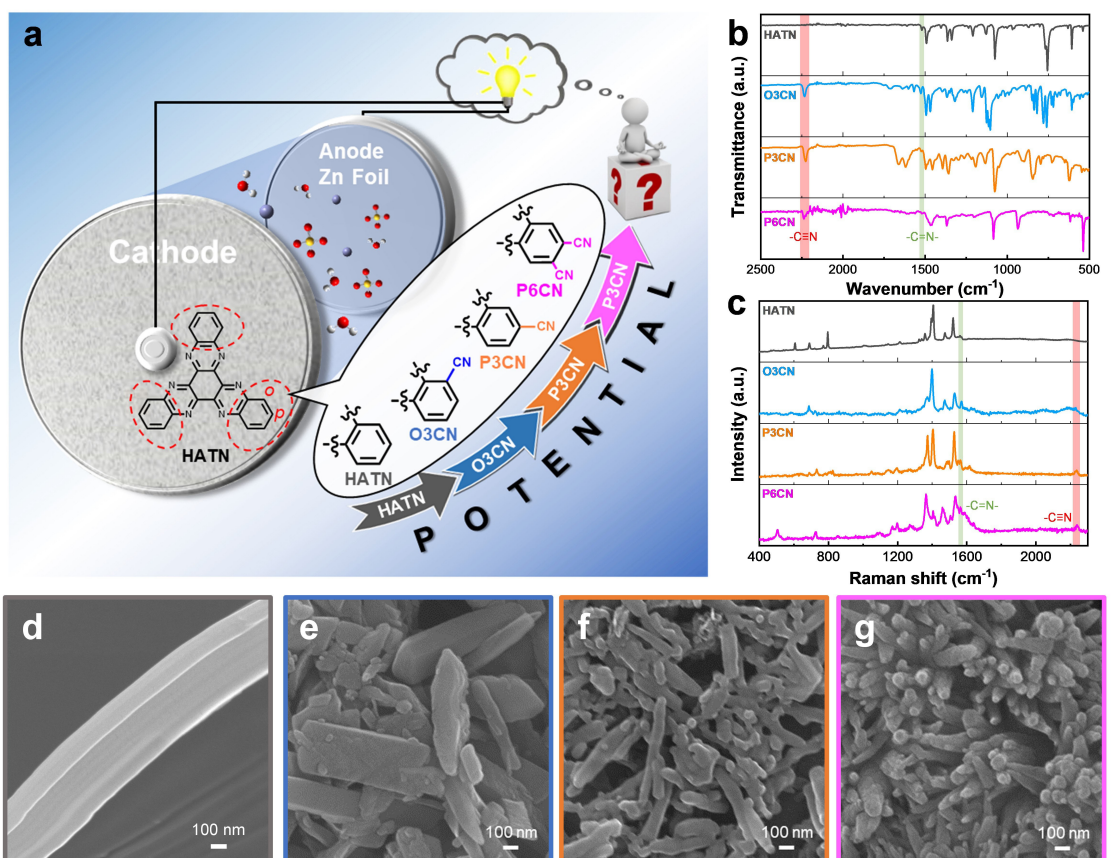


Figure 1. a) Effect mechanism of cyanide groups on the potential of aqueous zinc organic battery. b) FT-IR and c) Raman spectra of HATN (black), O3CN (blue), P3CN (orange), and P6CN (pink). SEM image of d) HATN, e) O3CN, f) P3CN, and g) P6CN.

like morphology, while P3CN and P6CN are rod-like with a diameter of about 100 nm. Interestingly, P6CN also formed micro-scale nanoclusters composed of nanorods.

To confirm the effect of -CN on the energy levels and band gap of the structures from the theoretical, the HOMO and LUMO energy levels of HATN, O3CN, P3CN, and P6CN were calculated by the DFT method (Figures 2a and S11). Compared with HATN, the HOMO levels of O3CN, P3CN, and P6CN are reduced by -0.36 , -0.36 , and -0.69 eV, respectively, and the LUMO levels of O3CN, P3CN, and P6CN are reduced by -0.39 , -0.39 , and -0.71 eV, respectively. Although O3CN and P3CN may have different structures when synthesized, calculations show that their HOMO/LUMO energy levels are the same (Figure S11). The lower LUMO energy level possesses a higher electron affinity energy, which is beneficial to improve the ability to gain electrons. That is, the introduction of -CN makes it easier and faster for the cathode material to accept electrons during discharge, thus increasing the inherent reduction potential of the material. The band gaps of the three are tightened from 3.60 to 3.57 eV. The reduced band gap increases the electronic conductivity of the material, allowing them to own faster electron transmission. The improvements in these characteristics of electrode materials will affect the redox potential and reaction kinetics of the battery.

To further investigate the effect of introducing amounts and positions of -CN on the electrochemical properties, coin cells were assembled with these four materials as the cathodes, zinc foil as the anode, glass fiber as the separator, and 2 M zinc sulfate (ZnSO_4) solution as the electrolyte. As shown in Figures 2(b–e) and S12, the cyclic voltammetry (CV) tests of four materials are performed under a scan rate of 0.1 mV s^{-1} . It is well known that the reduction potential of electrode materials plays a decisive role in the discharge plateau of a

battery, thus the reduction peak positions of these four materials are mainly analyzed. As shown in Figure 2(f), all four reduction potentials of P6CN are higher than the corresponding potentials of HATN, indicating that the introduction of -CN can increase the overall reduction potential of the material.^[24] The reduction potential of P6CN is higher than that of both O3CN and P3CN, which indicates that the degree of increase in potential is positively correlated with the number of -CN. Interestingly, the potential of P3CN is higher than that of O3CN despite their equal number of the -CN, suggesting that the p-position is the better choice for increasing the potential when the number of the -CN is the same.

To further reveal the influence of the cyano group on energy storage, the battery performances of these four materials are investigated. Figures 3a and S13 describe the rate performances of O3CN, P3CN, and P6CN from 0.1 to 10 Ag^{-1} . The specific capacities of O3CN, P3CN, and P6CN at 0.1 Ag^{-1} are 190 , 280 , and 259 mAh g^{-1} , respectively, which achieved 54.3% , 80.0% , and 86.3% of their respective theoretical values. We note that the capacity of O3CN is far lower than the theoretical value, which may be caused by the steric effect (discussed in detail below).^[25] All three samples show excellent rate performance, especially P6CN can still reach the specific capacity of 220 mAh g^{-1} under the current density of 10 Ag^{-1} . This rate performance is better than most of the currently reported zinc organic cells (Figure S14), such as PTO,^[14] DTT,^[16] PANI,^[15] PBQS,^[26] C4Q,^[12] etc. In addition, the specific capacity of P3CN and P6CN increased slightly after 200 cycles at 0.3 Ag^{-1} (Figures S13c and 3b), while the capacity of HATN decreased gradually during the cycle (Figure S15a). We disassembled the batteries after cycling and photographed the separators and cathodes (Figure S16). It was found that the separator of HATN-based battery had a significant color change while these of

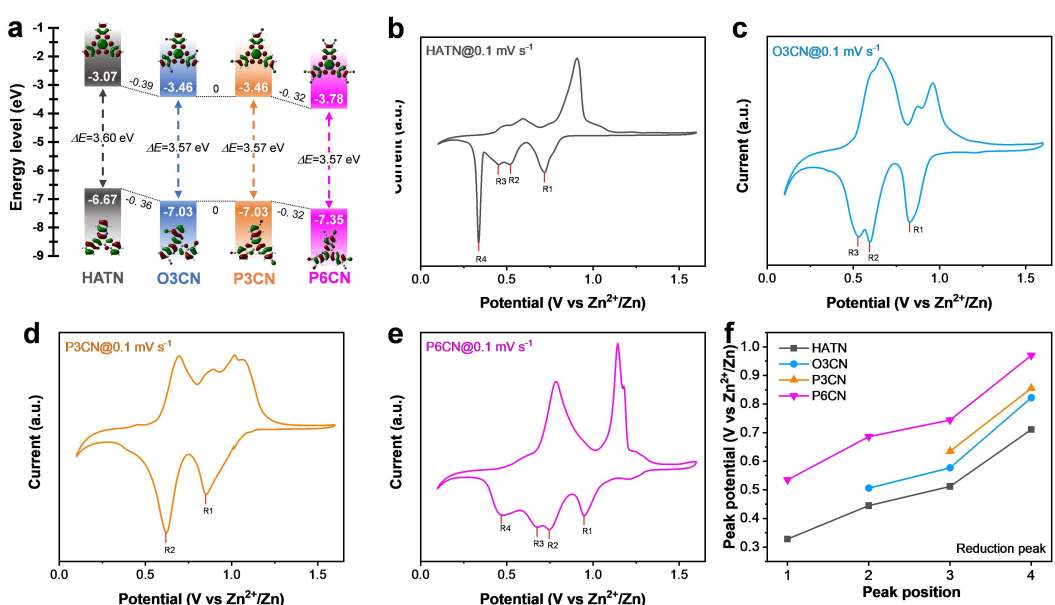


Figure 2. a) HOMO/LUMO energy levels and bandgaps of HATN, O3CN, P3CN, and P6CN calculated by DFT. CV curves of b) HATN, c) O3CN, d) P3CN, and e) P6CN. f) Comparison of reduction peak potentials of HATN, O3CN, P3CN, and P6CN.

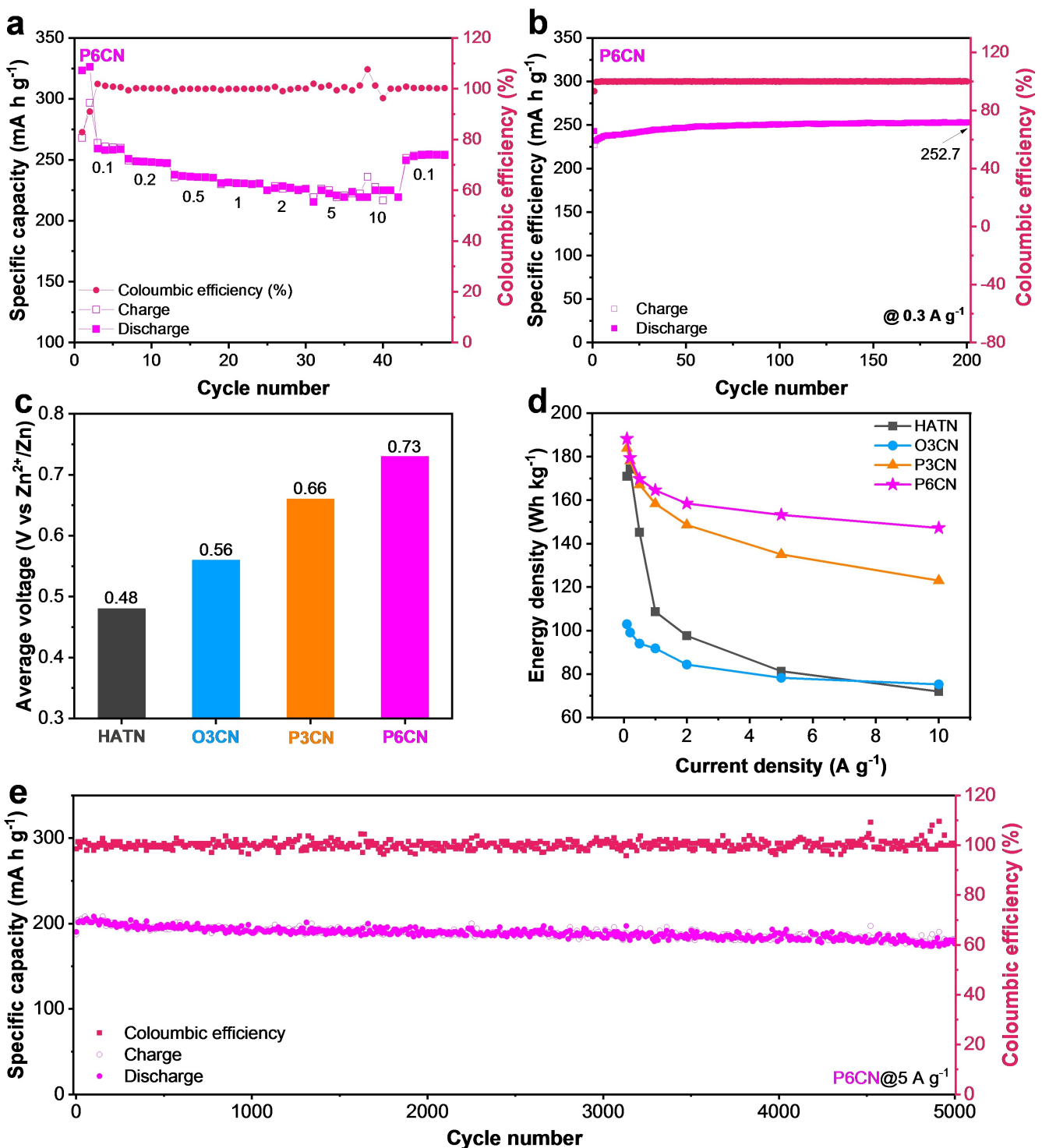


Figure 3. a) Rate capabilities of P6CN-based battery under current density from 0.1 to 10 A g^{-1} . b) The cycling performance of P6CN at 0.3 A g^{-1} . c) Comparison of the average voltages of HATN, O3CN, P3CN, and P6CN. d) Comparison of power density at various current density. e) Long-cycling performance of P6CN-based battery under 5 A g^{-1} .

other cells did not show this phenomenon. Therefore, the reason for the capacity decline may be that the HATN molecule is slightly soluble in water after discharge, while the introduction of the cyano group reduces the solubility of P3CN and

P6CN in water, thus improving the cycle stability under a low current density.^[27]

In order to clearly compare the effect of --CN on the voltage plateau, the galvanostatic charge-discharge (GCD) curves and

average working voltages of O3CN, P3CN, and P6CN at the 200th cycle were further dissected as shown in Figures S17, S18, and 3(c). Compared with HATN, the average discharge voltage of O3CN and P3CN containing three cyano groups increased by 0.08 V and 0.18 V, respectively. The cyano group at the p position has a greater influence on the average voltage, which is consistent with the conclusion of CV. More importantly, P6CN possesses the highest average discharge voltage of 0.73 V in the four materials, which is 0.25 V higher than that of HATN. It is worth noting that the average voltage of P6CN is only 0.07 V higher than that of P3CN, which indicates that the voltage cannot increase infinitely with the increase of the number of cyano groups, that is, the improvement of the voltage by cyano groups is limited. In addition, the power density under different current densities are calculated through the specific capacity and average voltage at corresponding rates (Figures 3d and S19). P6CN and P3CN show higher energy densities than HATN at each current density.^[20] Especially P6CN can still maintain 147 Wh kg⁻¹ at 10 Ag⁻¹, which benefits from higher specific capacity and improved average voltage. In general, P6CN is the structure with the best performance among the four materials. Therefore, its long-cycle performance under 5 Ag⁻¹ was further tested. The discharge capacity of P6CN can still maintain 180 mAh g⁻¹ after 5000 cycles (Figure 3e), and the Coulombic efficiency is close to 100% in this process. Comparing the cycle number and retained capacity of reported zinc organic ion batteries (Figure S20), the long-cycling stability of P6CN outperforms most organic electrode materials. In terms of mechanism, we prefer the reversible conversion reaction of the —C=N— bonds, which has been demonstrated by the characterization of ex situ FT-IR and H NMR.^[20] To investigate whether the cyano groups are involved in the conversion reaction, we performed ex situ FT-IR

characterizations of O3CN, P3CN, and P6CN in different charging/discharging states, respectively. As shown in Figure S21, —CN peaks were observed clearly for all three materials in different states, indicating that —CN was stable during the charging and discharging process and did not participate in the redox reaction.^[22]

To further understand the effect of cyano on the electrochemical properties, the DFT method was carried out for theoretical calculations. First, the optimal configurations of HATN, O3CN, P3CN, and P6CN at the lowest energy were resolved using water as the solvent model (Figures 4a and S22a).^[28] The side view results showed that all four materials maintained good flatness, which is attributed to the continuous conjugated rigid structure of the materials.^[20,22,29] HATNs present a triangular shape with the imine bond located in the center of the structure. To react with it, cations must pass through the side to reach the active site, so the channel width near the active sites determines the diffusion rate of ions to a certain extent and then affects the rate performance of the battery. The narrowest part of HATN is 6.09 Å by measuring the distance between two hydrogen atoms on the peripheral benzene ring. The channel width of P3CN and P6CN is the same as that of HATN, which is because the cyano group introduced by the p position is far from the active site and therefore does not have an effect on the channel width. Furthermore, the introduction of the cyano group increases the continuous conjugation of the main structure, which improves its electronic conductivity and facilitates rapid continuous electron transport. As a result, P3CN and P6CN can achieve excellent rate performance and a high percentage of theoretical specific capacity. In contrast, O3CN may appear in two conformations upon synthesis as shown in Figures 4(a) and S22, forming channels with two spacings of 5.27 and 4.47 Å.

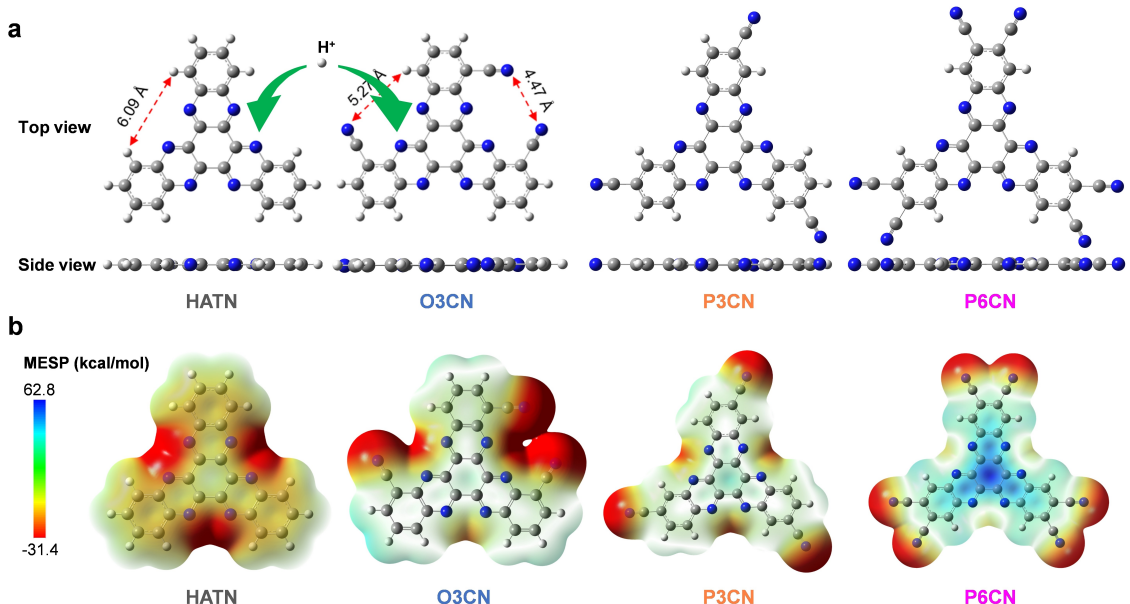


Figure 4. a) Top view and side view of the optimal configurations calculated by DFT. b) MESP distribution on the van der waals surface of molecules.

The smaller channels greatly limit the diffusion rate of ions, and thus the specific capacity of O3CN is the lowest among the four materials. In addition, the molecular electrostatic potentials (MESP) of HATN, O3CN, P3CN, and P6CN were further investigated. As shown in Figures 4(b) and S22(b), the blue region is the positive MESP value (more likely to attract nucleophilic reagents) and the red region is the negative MESP value (more likely to attract electrophilic reagents).^[30] In O3CN, P3CN, and P6CN, there is strong electronegativity around the cyano group. In addition, compared with HATN, cyano also changes the nucleophilic center (closer to the active site) of P6CN, which is conducive to the combination of electrons and electrode materials.

To further explore the essence of the excellent electrochemical performance of P6CN, the charge storage kinetics-related tests were researched. First, CVs with different scan rates are tested from 0.2 to 1 mV s⁻¹ (Figure 5a). With the increase in scanning speed, the strength of each redox peak increased significantly, while the peak position shifted slightly, implying that P6CN has excellent rate performance. Taking the redox peak currents and the corresponding scan rates, the *b* values [Figure 5b, calculated by Equation (1) in the Supporting Information] of the four reduction peaks are 0.821, 0.821, 0.867, and 0.864, respectively, indicating that the charge release process is mainly dominated by the fast surface-controlled.^[31] Interestingly, the *b* values of the three oxidation peaks are all below 0.75 (Figure S23), indicating that the charge storage process is affected by both diffusion-controlled and surface-controlled. The ratio of surface process contribution is further explored at the scan rates of 0.2 to 1 mV s⁻¹ by fitting *k*₁ and *k*₂ in Equation (2) of the Supporting Information. The results show that the surface-controlled increases gradually with the

increase of sweep speed, from 66.5% at 0.2 mV s⁻¹ to 88.3% at 0.8 mV s⁻¹ (Figure 5c). In particular, the non-diffusion-controlled process reached 92.1% when the scan rate increased to 1 mV s⁻¹ (Figure 5d). The high surface-control process ratio indicates that the surface/interface of the cathode material has fast reaction kinetics, which facilitates ion insertion/extraction, which is the reason for the excellent rate performance battery.^[22,32]

In addition, the electrochemical impedance spectrum (EIS) of the initial battery based on P6CN is displayed in Figure 5(e). The diameter of the semicircle at the high-frequency region is about 80 Ω, indicating that the P6CN-based battery has good conductivity and low charge transfer resistance.^[33] The oblique line in the low-frequency region shows a high slope, which reflects the fast ion mobility. To further investigate the ion diffusion coefficient of P6CN, the galvanostatic intermittent titration technique (GITT) was adopted by discharging/charging intermittently at the current of 0.05 A g⁻¹ for 15 min. The ion diffusion coefficient of P6CN is calculated by Equation (3) in the Supporting Information, and the value fluctuates in the range of 10⁻⁸ to 10⁻¹⁰ cm² s⁻¹ (Figure 5f). The P6CN shows a stable and fast ion diffusion coefficient in the early and middle stages of charge/discharge. The excellent ion mobility provides a prerequisite for rapid reaction kinetics,^[34] which further verifies the results of multi-sweep CV and EIS. To investigate the hydrophilicity of the electrode sheet in the electrolyte, the contact angles of the four materials were tested. As shown in Figure S24, the average contact angles of HATN, O3CN, P3CN, and P6CN are 71.2, 67.0, 60.1, and 56.9°, respectively. The results showed that the introduction of cyano groups greatly improved the affinity of the electrode for water, and the degree of improvement was positively correlated with the amount of

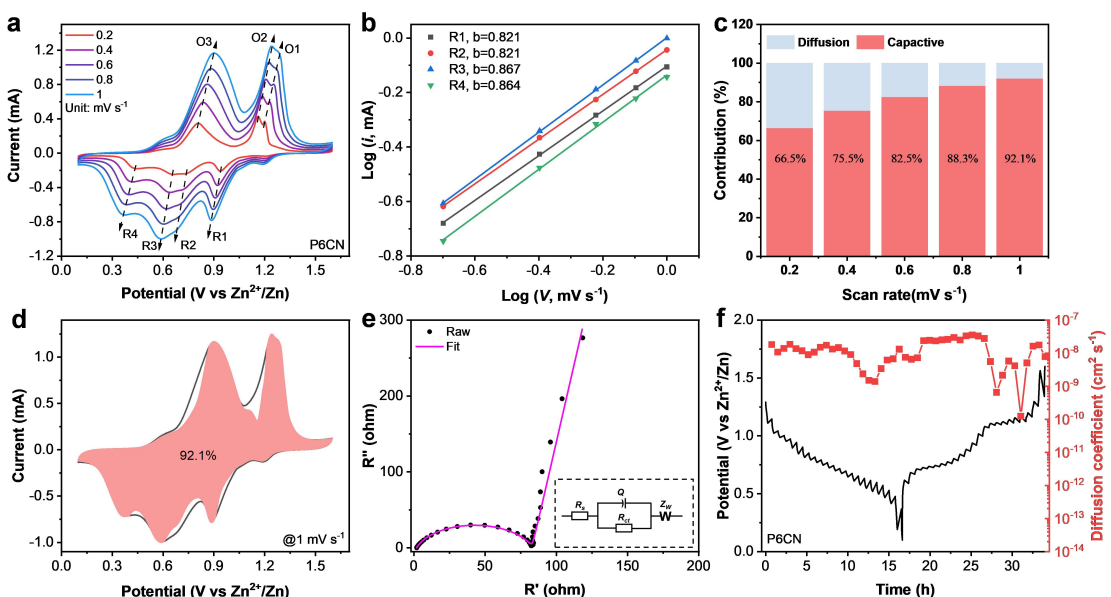


Figure 5. a) CV curves of P6CN at scan rates from 0.2 to 1 mV s⁻¹. b) The *b* values calculated from the reduction peaks of P6CN. c) Faradaic and non-faradaic contribution ratios of P6CN-based battery at various scan rates. d) Contribution ratios of surface-controlled process of P6CN at 1 mV s⁻¹. e) EIS spectrum of P6CN at initial state. f) The GITT and ion diffusion coefficient curves of P6CN.

—CN introduced. Furthermore, the self-discharge/charge measurements are an important method to detect the stability of the material in the battery.^[35] Therefore, the self-discharge/charge performances of batteries based on P6CN were further explored under the current density of 0.2 Ag^{−1}. As shown in Figure S25(a), P6CN showed a stable voltage curve in the 24 h rest after charging to 1.6 V. After the rest, the discharge capacity reached 243 mAh g^{−1}, which is almost consistent with the charge capacity. The same trend was obtained in the self-charge measurement (Figure S25b). These results show that the self-discharge capacity of the battery during rest can be negligible, which proves the remarkable stability of P6CN in the batteries.

Conclusion

In summary, we have synthesized three cyano-containing cathode materials based on HATN (named O3CN, P3CN, and P6CN, respectively) for the aqueous zinc-organic battery. The influence of the cyano group on the electrochemical performance is systematically discussed combined with various electrochemical measurements and DFT calculations. First, the introduction of the cyano group can improve the redox potential/average voltage of the battery, and the degree of improvement is proportional to the number of the cyano group. Secondly, when the number of the cyano group is the same, O3CN (o position) will produce the steric effect, reduce the diffusion rate of ions, and weaken the influence of the cyano group on potential, DFT calculation also proves this result. Compared with HATN (without the cyano group), the average voltage of P6CN increases from 0.48 V to 0.73 V (vs. Zn²⁺/Zn), which greatly improves the energy density of the battery. In addition, all three cathode materials containing cyano have good cycling stability at low/high current density, which is attributed to the introduction of cyano to reduce the solubility of the materials. As a result, the P6CN showed the best electrochemical performance and retained 88.2% of the initial capacity after 5000 cycles at 5 Ag^{−1}. This study attempts to elucidate the intrinsic relationship between the introduction location and the number of the cyano group with the electrochemical performance, which will provide a research basis for improving the voltage of organic cathode materials in the future.

Experimental Section

The detailed synthesis, electrode preparation process, and test conditions are shown in the SI.

Acknowledgements

This work was supported by the National Natural Science Foundation of China (U1804253, 52172231, 51972259), the Natural Science Foundation of Hubei Province (2022CFA087),

Industrialization Project of Xiangyang Technology Transfer Center of Wuhan University of Technology (WXCJ-20220017), and the Fundamental Research Funds for the Central Universities (WUT: 2020III043GX, 2020III015GX).

Conflict of Interest

The authors declare no conflict of interest.

Data Availability Statement

The data that support the findings of this study are available in the supplementary material of this article.

Keywords: zinc-organic batteries • organic cathodes • cyano groups • redox potentials • average voltages

- [1] a) H. Li, Z. X. Wang, L. Q. Chen, X. J. Huang, *Adv. Mater.* **2009**, *21*, 4593; b) B. Dunn, H. Kamath, J. M. Tarascon, *Science* **2011**, *334*, 928; c) X. Y. Cao, J. B. Liu, L. M. Zhu, L. L. Xie, *Energy Technol.* **2019**, *7*; d) L. M. Zhu, G. C. Ding, L. L. Xie, X. Y. Cao, J. P. Liu, X. F. Lei, J. X. Ma, *Chem. Mater.* **2019**, *31*, 8582.
- [2] J. Liu, W. Zhou, R. Zhao, Z. Yang, W. Li, D. Chao, S. Z. Qiao, D. Zhao, *J. Am. Chem. Soc.* **2021**, *143*, 15475.
- [3] a) J. Huang, Z. Wang, M. Hou, X. Dong, Y. Liu, Y. Wang, Y. Xia, *Nat. Commun.* **2018**, *9*, 2906; b) F. Wan, L. Zhang, X. Dai, X. Wang, Z. Niu, J. Chen, *Nat. Commun.* **2018**, *9*, 1656; c) X. Jia, C. Liu, Z. Neale, J. Yang, G. Cao, *Chem. Rev.* **2020**, *120*, 7795.
- [4] a) P. He, M. Yan, G. Zhang, R. Sun, L. Chen, Q. An, L. Mai, *Adv. Energy Mater.* **2017**, *7*, 1601920; b) W. Li, K. Wang, S. Cheng, K. Jiang, *Adv. Energy Mater.* **2019**, *9*, 1900993; c) J. Hao, X. Li, S. Zhang, F. Yang, X. Zeng, S. Zhang, G. Bo, C. Wang, Z. Guo, *Adv. Funct. Mater.* **2020**, *30*, 2001263.
- [5] S. Tan, F. Xiong, J. Wang, Q. An, L. Mai, *Mater. Horiz.* **2020**, *7*, 1971.
- [6] D. Chao, S.-Z. Qiao, *Joule* **2020**, *4*, 1846.
- [7] a) F. Xiong, S. Tan, X. Yao, Q. An, L. Mai, *Mater. Today* **2021**, *45*, 169; b) Y. Lu, J. Chen, *Nat. Chem. Rev.* **2020**, *4*, 127.
- [8] a) L. L. Wang, K. W. Huang, J. T. Chen, J. R. Zheng, *Sci. Adv.* **2019**, *5*, eaax4279; b) N. Wang, C. Sun, X. Liao, Y. Yuan, H. Cheng, Q. Sun, B. Wang, X. Pan, K. Zhao, Q. Xu, X. Lu, J. Lu, *Adv. Energy Mater.* **2020**, *10*, 2002293; c) J. H. Jo, Y. Aniskevich, J. Kim, J. U. Choi, H. J. Kim, Y. H. Jung, D. Ahn, T. Y. Jeon, K. S. Lee, S. H. Song, H. Kim, G. Ragoisha, A. Mazanik, E. Streltsov, S. T. Myung, *Adv. Energy Mater.* **2020**, *10*, 2001595.
- [9] a) W. Sun, F. Wang, S. Hou, C. Yang, X. Fan, Z. Ma, T. Gao, F. Han, R. Hu, M. Zhu, C. Wang, *J. Am. Chem. Soc.* **2017**, *139*, 9775; b) B. Wu, G. Zhang, M. Yan, T. Xiong, P. He, L. He, X. Xu, L. Mai, *Small* **2018**, *14*, e1703850; c) N. Zhang, F. Cheng, J. Liu, L. Wang, X. Long, X. Liu, F. Li, J. Chen, *Nat. Commun.* **2017**, *8*, 405.
- [10] a) Z. Li, T. Liu, R. Meng, L. Gao, Y. Zou, P. Peng, Y. Shao, X. Liang, *Energy Environ. Mater.* **2020**, *4*, 111; b) Y. Zeng, J. Xu, Y. Wang, S. Li, D. Luan, X. D. Lou, *Angew. Chem. Int. Ed.* **2022**, DOI: 10.1002/anie.20221203110.1002/anie.202212031; c) Y. Zeng, X. F. Lu, S. L. Zhang, D. Luan, S. Li, X. W. D. Lou, *Angew. Chem. Int. Ed.* **2021**, *60*, 22189.
- [11] Z. Tie, Z. Niu, *Angew. Chem. Int. Ed.* **2020**, *59*, 21293.
- [12] Q. Zhao, W. Huang, Z. Luo, L. Liu, Y. Lu, Y. Li, L. Li, J. Hu, H. Ma, J. Chen, *Sci. Adv.* **2018**, *4*, eaao1761.
- [13] D. Kundu, P. Oberholzer, C. Glaros, A. Bouzid, E. Tervoort, A. Pasquarello, M. Niederberger, *Chem. Mater.* **2018**, *30*, 3874.
- [14] Z. Guo, Y. Ma, X. Dong, J. Huang, Y. Wang, Y. Xia, *Angew. Chem. Int. Ed.* **2018**, *57*, 11737.
- [15] H. Y. Shi, Y. J. Ye, K. Liu, Y. Song, X. Sun, *Angew. Chem. Int. Ed.* **2018**, *57*, 16359.
- [16] Y. Wang, C. Wang, Z. Ni, Y. Gu, B. Wang, Z. Guo, Z. Wang, D. Bin, J. Ma, Y. Wang, *Adv. Mater.* **2020**, *32*, 2000338.

- [17] Y. Gao, G. Li, F. Wang, J. Chu, P. Yu, B. Wang, H. Zhan, Z. Song, *Energy Storage Mater.* **2021**, *40*, 31.
- [18] Y. An, Y. Liu, S. Tan, F. Xiong, X. Liao, Q. An, *Electrochim. Acta* **2022**, *404*, 139620.
- [19] W. Wang, V. S. Kale, Z. Cao, Y. Lei, S. Kandambeth, G. Zou, Y. Zhu, E. Abouhamad, O. Shekhah, L. Cavallo, M. Eddaoudi, H. N. Alshareef, *Adv. Mater.* **2021**, *33*, e2103617.
- [20] Z. Tie, L. Liu, S. Deng, D. Zhao, Z. Niu, *Angew. Chem. Int. Ed.* **2020**, *59*, 4920.
- [21] Y. Chen, J. Li, Q. Zhu, K. Fan, Y. Cao, G. Zhang, C. Zhang, Y. Gao, J. Zou, T. Zhai, C. Wang, *Angew. Chem. Int. Ed.* **2022**, *61*, e202116289.
- [22] Z. Ye, S. Xie, Z. Cao, L. Wang, D. Xu, H. Zhang, J. Matz, P. Dong, H. Fang, J. Shen, M. Ye, *Energy Storage Mater.* **2021**, *37*, 378.
- [23] M. S. Wu, N. T. H. Luu, T. H. Chen, H. Lyu, T. W. Huang, S. Dai, X. G. Sun, A. S. Ivanov, J. C. Lee, I. Popovs, W. Kaveevivitchai, *Adv. Energy Mater.* **2021**, *11*, 2100330.
- [24] K. Nakashima, T. Shimizu, Y. Kamakura, A. Hinokimoto, Y. Kitagawa, H. Yoshikawa, D. Tanaka, *Chem. Sci.* **2020**, *11*, 37.
- [25] J. Wang, C. S. Chen, Y. Zhang, *ACS Sustainable Chem. Eng.* **2017**, *6*, 1772.
- [26] G. Dawut, Y. Lu, L. Miao, J. Chen, *Inorg. Chem. Front.* **2018**, *5*, 1391.
- [27] J. Kumankuma-Sarpong, S. Tang, W. Guo, Y. Fu, *ACS Appl. Mater. Interfaces* **2021**, *13*, 4084.
- [28] J. Tomasi, B. Mennucci, R. Cammi, *Chem. Rev.* **2005**, *105*, 2999.
- [29] C. Peng, G.-H. Ning, J. Su, G. Zhong, W. Tang, B. Tian, C. Su, D. Yu, L. Zu, J. Yang, M.-F. Ng, Y.-S. Hu, Y. Yang, M. Armand, K. P. Loh, *Nat. Energy* **2017**, *2*, 17074.
- [30] C. Wu, M. Hu, X. Yan, G. Shan, J. Liu, J. Yang, *Energy Storage Mater.* **2021**, *36*, 347.
- [31] Y. Liu, M. Huang, F. Xiong, J. Zhu, Q. An, *Chem. Eng. J.* **2022**, *428*, 131092.
- [32] T. Sun, Z. J. Li, Y. F. Zhi, Y. J. Huang, H. J. Fan, Q. Zhang, *Adv. Funct. Mater.* **2021**, *31*, 2010049.
- [33] N. Wang, R. Zhou, H. Li, Z. Zheng, W. Song, T. Xin, M. Hu, J. Liu, *ACS Energy Lett.* **2021**, *6*, 1141.
- [34] S. Zheng, D. Shi, D. Yan, Q. Wang, T. Sun, T. Ma, L. Li, D. He, Z. Tao, J. Chen, *Angew. Chem. Int. Ed.* **2022**, *61*, e202117511.
- [35] H. Zhang, S. Xie, Z. Cao, D. Xu, L. Wang, H. Fang, J. Shen, M. Ye, *ACS Appl. Energ. Mater.* **2021**, *4*, 655.

Manuscript received: October 23, 2022

Revised manuscript received: December 1, 2022

Accepted manuscript online: December 7, 2022

Version of record online: December 20, 2022